Simulation of the generation of high-power pulses in the GHz range with three-section DBR lasers

K.-H. Hasler, H. Wenzel, A. Klehr and G. Erbert

Abstract: The dynamical behaviour of three-section distributed Bragg reflected (DBR) lasers containing an active gain section and passive phase-shift and Bragg-grating sections was studied and modelled by numerically solving the travelling wave equations and a rate equation for the carrier density. By changing the parameters determining the optical gain or absorption, respectively, in the phase section a switching behaviour, hysteresis phenomena and self-sustained pulsations were obtained. By injecting small current pulses through the phase section, high-power optical pulses with small spectral width and repetition rates in the GHz range were generated. Experimentally, this was achieved by a selective heating of the phase section and by modulating the current injected into the phase section. In contrast to DBR lasers emitting at 1.3 μm and 1.55 μm, in the DBR lasers under investigation with an emission wavelength of 1.06 μm the active layer extends over all sections. Thus by the heating the interband absorption in the active layer of the phase section is strongly increased, while owing to the current pulses the absorption is rapidly reduced. Thus, giant light pulses are emitted which have a small spectral width owing to the wavelength selectivity of the Bragg grating.

1 Introduction

High-power optical pulses with small spectral width and repetition rates in the GHz range are required for several applications, such as free space optical communication or frequency conversion. Usually, optical pulses can be obtained by active or passive Q-switching, gain switching or mode locking. Q-switching can be achieved either by changing the absorption within the cavity (absorptive type) [1] or by changing the wavelength-dependent feedback of a Bragg reflector (dispersive type) [2]. In the case of absorptive Q-switching, which yields the highest peak powers, saturable absorbers are introduced into the cavity of Fabry–Perot (FP) lasers. One disadvantage of this approach is the large spectral width of the pulses because there is no wavelength-selective feedback.

We present a new possibility of realising high-power pulses by an absorptive Q-switching of distributed Bragg reflector (DBR) lasers with an emission wavelength of 1.06 μm, containing gain, phase-shift and Bragg-grating sections. The passive phase-shift and Bragg-grating sections can be selectively heated. In contrast to DBR lasers emitting at 1.3 or 1.55 μm, the active layer extends over all sections. Thus, the interband absorption within the active layer of the passive sections can directly act as a saturable absorber necessary for Q-switching. There is no need to introduce additional absorbers. By selectively heating the phase section the interband absorption can be increased there and different modes of operation (switching, self-sustained pulsations, pulse generation) can be established. Moreover, by injecting a small current through the p-n junction of the phase section the absorption can be decreased very quickly which opens up the possibility of generating short optical pulses with high peak power at a desired repetition rate. The small spectral width is a consequence of the wavelength selectivity of the internal Bragg grating.

Numerical simulation of self-sustained pulsations in semiconductor lasers caused by saturable absorbers is mostly performed with a rate equation approach [3]. For a recent review we refer to [4]. In contrast, we use a general-purpose mixed frequency-time domain simulation program based on the numerical solution of the travelling wave equations and the carrier density rate equation [5]. It allows accurate calculation of the spatio-temporal behaviour and the optical spectrum of semiconductor lasers consisting of an arbitrary number of different sections.

2 Principle of switching behaviour and pulse generation

The three-section DBR laser investigated experimentally and theoretically is depicted in Fig. 1. It consists of an active gain section and passive phase and Bragg sections with lengths of $L_g = 1000$ μm, $L_{ph} = 300$ μm and $L_{DBR} = 700$ μm, respectively. Details of the structure can be found in [6–8]. The laser emits at 1060 nm and has a ridge waveguide for lateral optical confinement. The active layer consists of a compressively strained InGaAs quantum well (QW) embedded in tensile-strained GaAsP spacer layers and GaAs waveguides. In contrast to DBR lasers emitting at 1.3 or 1.55 μm [6], the active layer extends over all sections. Thus, the optical loss in the passive sections owing to interband absorption can be minimised

IEE Proceedings online no. 20020505

DOI: 10.1049/ip-opt:20020505

Paper first received 29th January and in revised form 1st May 2002

The authors are with the Ferdinand-Braun-Institut für Höchstfrequenztechnik, Albert-Einstein-Straße 11, 12489 Berlin, Germany

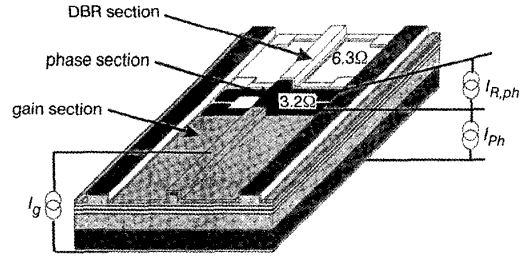

Fig. 1 *Schematic view of the three-section DBR laser emitting at $\lambda = 1060$ nm*

The epitaxial layers including the active InGaAs QW extend over all sections

or maximised depending on the detuning between Bragg wavelength and peak gain wavelength.

The ridge waveguides of the passive sections are covered with very narrow TiPtAu metal stripes of a width of 10 μm, having ohmic resistances of $R_{ph} = 3.2\ \Omega$ and $R_{DBR} = 6.3\ \Omega$ for the phase section and Bragg section, respectively. Selective heating of these two sections can be achieved by varying the current $I_{R,ph}$ and $I_{R,DBR}$ through the resistors. In addition, currents I_{ph} and I_{DBR} can be injected into the passive sections by applying a forward bias between the top metal stripes and the bottom contact acting as ohmic p- and n-contacts, respectively. By a proper moderate heating of the phase and Bragg sections the emission wavelength of the DBR laser can be tuned by about 300 GHz owing to the thermally induced refractive index change [7]. In this paper, we investigate the effect of strong interband absorption in the phase section owing to strong heating.

First, the influence of a rise of the heat sink temperature T_s from 25 °C to 55 °C on the light-current (L–I) characteristic can be seen in Fig. 2. At $T_s = 25$ °C, the laser has a threshold current of about 30 mA. No such threshold can be observed at $T_s = 55$ °C. Instead, with increasing current I_g the laser turns suddenly on to a power level of 45 mW at a current $I_g = 122$ mA. With further increase of I_g the L–I curve exhibits almost the same slope as without heating. By decreasing I_g the laser turns off at a smaller current of $I_g = 93$ mA. Thus, a hysteresis phenomenon is observed.

The influence of selective heating of the phase section can be seen in Fig. 3. Here, the gain section is biased with 130 mA corresponding to an output power of nearly

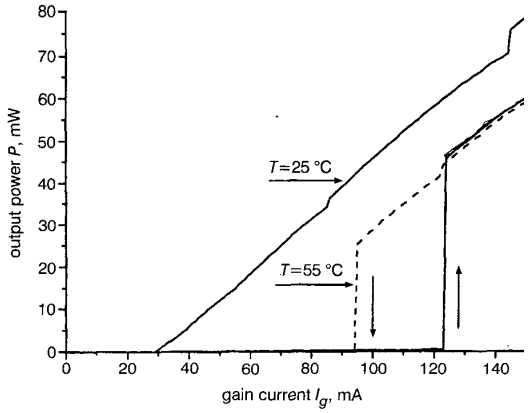

Fig. 2 *Measured output power P against current I_g through the gain section for two temperatures of the heat sink*

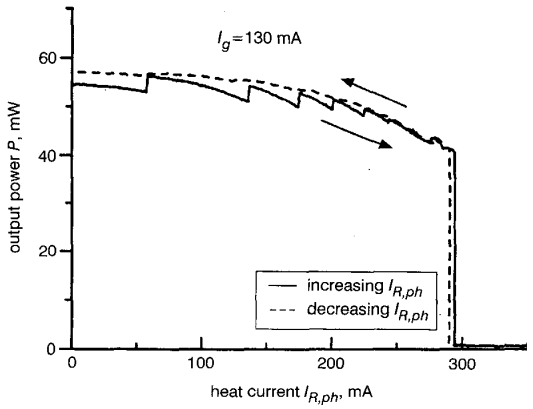

Fig. 3 *Measured output power P against current $I_{R,ph}$ through the resistor of the phase section*

55 mW for $I_{R,ph} = 0$. With increasing $I_{R,ph}$, i.e. temperature in the phase section, the output power decreases slightly and power jumps owing to longitudinal mode hopping occur. For $I_{R,ph} = 295$ mA the power decreases to the luminescence level, i.e. the laser is turned off. With decreasing current $I_{R,ph}$ the laser is turned on at a slightly smaller current, i.e. a small hysteresis can be found again.

The observed behaviour can be explained by a strong change of the saturable interband absorption in the QW of the passive sections of the laser with temperature. Fig. 4 shows the calculated imaginary part of the dielectric function ε of the InGaAs QW in the active gain section for an excess carrier density of $N = 2 \times 10^{18}$ cm^{-3} (Im ε is proportional to the optical gain coefficient) and in the passive phase section (Im ε is proportional to the absorption coefficient) with and without heating. The lasing wavelength (defined by the Bragg period) is located at the long wavelength side of the gain spectrum and for $T = 300$ K the absorption in the passive sections is small. However, a temperature rise to $T = 350$ K in the phase section leads to a red shift of the absorption edge owing to the narrowed bandgap, and the absorption at the lasing wavelength increases strongly. By injecting or generating

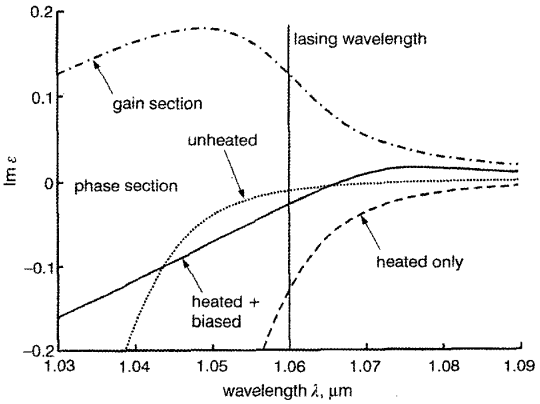

Fig. 4 *Calculated imaginary part of the dielectric function of the InGaAs QW caused by interband transitions against wavelength*

Gain section: $N = 2 \times 10^{18}$ cm^{-3}, $T = 300$ K
Phase section: $N = 0$, $T = 300$ K (unheated); $N = 0$, $T = 350$ K (heated only); $N = 1.25 \times 10^{18}$ cm^{-3}, $T = 350$ K (heated + biased). The lasing wavelength is denoted by a vertical line

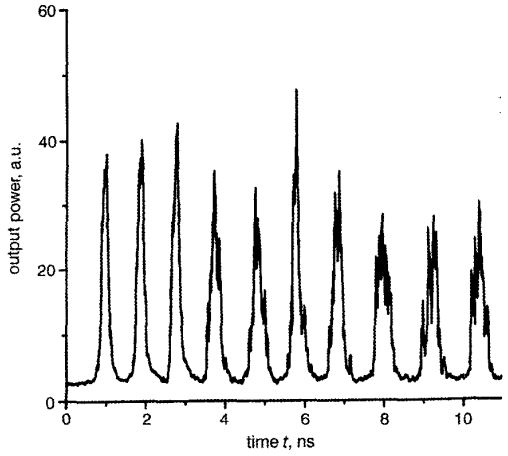

Fig. 5 *Measured self-sustained pulsation*
$T_s = 50\,°C$, $I_g = 200$ mA, $I_{R,ph} = 387$ mA

excess carriers in the heated phase section the absorption can be decreased again.

The increase of the absorption caused by heating leads exactly to the experimentally observed turning off of the laser while the temporary decrease of the absorption caused by injecting a small current pulse through the p-n junction leads to a very fast turning on of the laser and therefore to the generation of a light pulse. Since at high temperatures lasing is suppressed even for large currents through the gain section, the generation of giant light pulses should be possible. Additionally, as for every saturable absorber, self-sustained pulsation due to absorptive self-Q-switching can be expected.

Fig. 5 shows self-sustained pulsation with a repetition frequency of nearly 1 GHz observed at a temperature of the phase section just before turning off of the laser. In Fig. 6 the phase section is heated so strongly that even for large currents through the gain section no lasing is observed. By injecting small current pulses into the phase section optical pulses with a peak power of more than 600 mW and a full width at half maximum (FWHM) of less than 60 ps are generated.

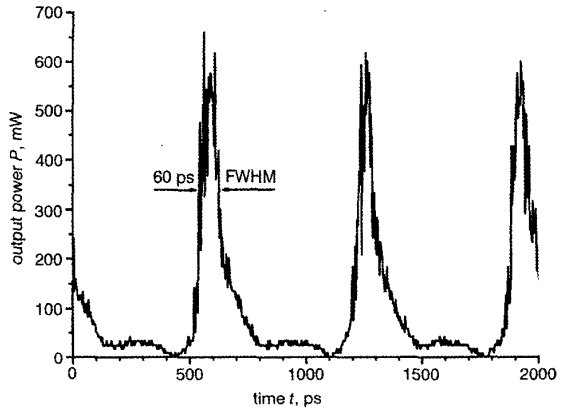

Fig. 6 *Optical pulses generated by small sinusoidal current pulses through the phase section with a repetition frequency of 1.5 GHz*
$T_s = 50\,°C$, $I_g = 300$ mA, $I_{R,ph} = 205$ mA

To finish this Section we remark that the advantage of using a three-section DBR laser for the pulse generation in comparison to a multi-section Fabry–Perot laser is that the lasing wavelength is fixed by the Bragg grating. Therefore it is possible to realise strongly different differential gain values $g_{diff} = \partial g/\partial N$ in the gain and phase sections ($g_{diff}^{gain} \ll g_{diff}^{phase}$) which is crucial for self-sustained pulsations. Additionally, the Bragg grating reduces the number of simultaneously lasing longitudinal modes during the pulse owing to the finite bandwidth of the reflectivity spectrum.

3 Model and simulation

To understand the spatio-temporal behaviour of the device and to optimise the longitudinal structure with respect to peak power, width, repetition rate and chirp of the generated pulses it is necessary to perform numerical simulations. So far most of the existing models for absorptive-Q-switched lasers are based on a rate equation approach [3], which does not resolve the spatial behaviour inside the laser and also does not allow us to calculate, for instance, the optical spectrum.

There are several methods for modelling the spatial-longitudinal and temporal behaviour of multisection FP, distributed feedback (DFB) and DBR lasers. Most of the existing models, which were developed to simulate lasers for telecommunication applications, are based on the solution of the time-dependent coupled wave equation using the transfer-matrix method [9], power matrix method [10], transmission line method [11] or finite difference approaches [12, 13]. Our calculations are based on a finite difference solution of the equations in the time domain and are also compared with a transfer matrix approach. Detailed descriptions can be found in [5] and [14]. We will describe the basic equations briefly.

3.1 Travelling wave equations

The optical field within the laser, assumed to be TE-like polarised, is decomposed into two counter-propagating waves along the longitudinal axis:

$$E(x, y, z, t) = A(x, y)(\boldsymbol{\Psi}^{+}(z, t)e^{-i\beta_0 z} + \boldsymbol{\Psi}^{-}(z, t)e^{i\beta_0 z})e^{i\omega_0 t} \quad (1)$$

where $A(x, y)$ describes the transverse mode distribution which is assumed to be known. The rapidly varying dependences with respect to the longitudinal axis z and time t are separated by the introduction of a reference propagation factor β_0 (equal to the Bragg wave number) and an optical reference frequency ω_0 (corresponding to the vacuum reference wavelength λ_0). The slowly varying amplitudes $\boldsymbol{\Psi}^{\pm}(z, t)$ obey the well-known travelling wave equations (TWEs) [15]

$$-\frac{i}{v_g}\frac{\partial \boldsymbol{\Psi}^{\pm}}{\partial t} = \pm i\frac{\partial \boldsymbol{\Psi}^{\pm}}{\partial z} - \Delta\beta(N, P)\boldsymbol{\Psi}^{\pm} - \kappa^{\mp}\boldsymbol{\Psi}^{\mp} + F_{sp}^{\pm} \quad (2)$$

The group velocity v_g and the coupling coefficients $\kappa^{\mp}$ of the Bragg grating are constant within each section. For a first order index grating $\kappa^{-} = \kappa^{*+}$ holds, where the asterisk denotes complex conjugation.

For the relative complex propagation factor $\Delta\beta(N, P)$ we use

$$\Delta\beta(N, P) = -i\frac{\alpha}{2} + \frac{(i + \alpha_H)}{2}g(N, P) \quad (3)$$

with a linear dependence of the modal optical gain of the active quantum well on the excess carrier density $N(z, t)$

$$g = \frac{g_{diff}(N - N_{tr})}{1 + \varepsilon(\lambda_0 L / v_g hcV) P} \tag{4}$$

The parameters α, α_H, g_{diff} and N_{tr} represent the internal optical losses, Henry's linewidth enhancement factor, the differential gain and the transparency carrier density, respectively. In (4), ε is the gain compression factor, L is the sectional length and V the volume of the active region, h is Planck's constant and c is the velocity of light. The optical power is given by

$$P = |\Psi^+|^2 + |\Psi^-|^2 \tag{5}$$

The quantities $F_{sp}^{\pm}$ in (2) represent the Langevin noise sources due to spontaneous emission. They are also necessary to avoid a numerical underflow if the laser is turned off. The TWEs represent hyperbolic partial differential equations. They have to be completed by initial and boundary conditions. We use the usual reflective boundary conditions for the optical fields at the facets (reflectivities R_f and R_r) [15]. Solutions from a preceding simulation, for example, are taken as initial conditions.

3.2 Carrier density rate equation

The travelling wave equations are coupled via the optical power to the carrier-density rate equation [15, 16] for the kth section:

$$\frac{dN}{dt} = \frac{I_k}{eV_k} - \frac{dU_F/dN}{eV_k R} \Delta N_k - \left(\frac{N}{\tau_{nr}} + BN^2 + CN^3\right) - \frac{\lambda_0 L_k}{hcV_k} g_k P \tag{6}$$

where I_k is the current injected into the kth section and R and U_F represent the series resistance and the Fermi voltage, respectively. The term $\Delta N_k = \overline{N}_k - N$ describes the deviation of the continuously varying carrier density from its average value within the kth section. If R goes to zero, ΔN_k must approach zero, too, which means a complete suppression of spatial holeburning. In the following, we will omit the index k throughout. The non-radiative and spontaneous radiative recombination is described by the third term (within the parentheses) on the right hand side. The last term is the stimulated radiative recombination term proportional to the product of optical gain and power. In the passive sections where the optical gain is usually negative this term describes actually the generation of excess carriers owing to the absorption of photons. The carrier density depends on the longitudinal axis z, because I_k may differ from section to section (this leads to different, but constant, carrier densities in every section) and because the local optical power depends on z via the TWEs (2) (this leads to a continuously varying carrier density in every section).

The action of the selective heating of the passive sections is modelled by an appropriate change of the gain parameters transparency density N_{tr} and modal differential gain g_{diff}. With increasing temperature the bandgap energy decreases. On the other hand, the lasing wavelength remains constant because it is determined by the Bragg period of the unheated DBR section. It is known [17] that the differential gain increases if the spacing between photon and bandgap energies gets larger. The transparency density increases, too. The actual dependences of these gain parameters on the heating currents are difficult to calculate, because one has to determine the distribution of the temperature and the electrostatic potential depending on the excess carrier densities within the device, coupled to a microscopic gain model including many-body corrections. Therefore, we used N_{tr} and g_{diff} merely as fitting parameters, in order to obtain the experimentally observed behaviour at roughly the same injection currents. The other parameters were held constant.

Finally we remark that we neglected any thermal crosstalk between the sections. Thermal simulations of a two-section DFB laser, where only one section is electrically pumped, yielded a transition region of only 30 μm, where the temperature drops to 10% of its value in the heated section [18].

3.3 Numerical schemes

The coupled differential equations are numerically solved by the computer code LDSL developed at WIAS and HU Berlin [5]. In the LDSL code two different numerical schemes can be used to solve the differential equations. The first one is based on the transfer matrix method (TMM) for the TWEs (1) as described in [16] combined with the forward Euler method for the carrier rate equation (6). Another method is a finite difference scheme of the predictor–corrector type (FDPC) for solving the equations. Both numerical schemes yield almost the same results. The FDPC has some advantages with respect to the numerical stability at high gain currents and the TMM has some advantages with respect to a smaller high-frequency numerical noise. In both schemes, the ratio of the discretisation steps in space and time is given by the group velocity. We used an equidistant longitudinal discretisation step of $\Delta z = 10$ nm which results in a temporal discretisation step of $\Delta t = 126.6$ fs which is a compromise

Table 1: Some essential parameters of the simulations

Parameter	Symbol	Values
Length of gain section	L_g	1000 μm
Length of phase section	L_{ph}	300 μm
Length of DBR section	L_{DBR}	700 μm
Ridge width	W	5 μm
QW thickness	d	8 nm
Reflectivity front facet	R_f	0.1
Reflectivity rear facet	R_r	0.01
Coupling coefficient	$\kappa^+ = \kappa^-$	70 cm^{-1}
Non-radiative recombination lifetime	τ_{nr}	1 ns
Radiative recombination coefficient	B	2×10^{-10} cm^3 s^{-1}
Auger recombination coefficient	C	0
Differential gain (unheated)	g_{diff}	2.4×10^{-17} cm^2
Carrier density for transparency (unheated)	N_{tr}	8×10^{17} cm^{-3}
Gain compression factor	ε	0.3×10^{-19} cm^3, 0.5×10^{-19} cm^3
Henry's α-factor	α_H	−1.3
Group index	$n_g = c/v_g$	3.8
Internal optical losses	α	5 cm^{-1}

between sufficient accuracy and moderate simulation time. Note that the photon round-trip time is about 50 ps for the 2 mm long devices. In order to improve the numerical stability and to obtain smooth solutions, i.e. to minimise high-frequency numerical noise, a digital filter is used [5, 16].

The basic parameters used in the simulations are listed in Table 1.

4 Stationary simulation results

We simulated the stationary behaviour by starting below threshold with a very small constant optical power within the cavity, and then by increasing the current I_g in steps of 0.1–10 mA (the smaller steps are taken near the threshold or near jumps in the L–I characteristic), where the solution of the preceding step was taken as the initial condition. A similar procedure was chosen for a decreasing current. For each current, the temporal evolution of the output power was traced until the relaxation oscillations were sufficiently damped (typically after 5 ns).

Fig. 7 shows the calculated L–I characteristics for both unheated and heated phase sections. In the latter case the differential gain was $g_{diff} = 1.25 \times 10^{-16}$ cm^2 and the carrier density for transparency was $N_{tr} = 2.5 \times 10^{18}$ cm^{-3}. 3. We find a similar switching behaviour to that found experimentally (compare with Fig. 2): an abrupt turn on/off, almost the same slope of the L–I curve with and without heating, and hysteresis.

The calculated currents are somewhat smaller than the experimental ones. The reason is that in the simple spatial one-dimensional model several effects such as current spreading, carrier diffusion and leakage current are neglected. Roughly, we have to multiply all currents by a factor of 1.6 (ratio of the threshold currents). This makes it possible to relate the heating parameters g_{diff} and N_{tr} of the computer model to the heating currents and temperatures in the experiment.

Next, we varied g_{diff} and N_{tr} in the phase section over a large range and investigated the behaviour of the laser for different currents I_g. Increasing values for N_{tr} and g_{diff} correlate with increasing values of the temperature. In general, three regions of operation can be distinguished. For small values of N_{tr} and g_{diff} stable laser emission can be found, i.e. the laser is 'on'. For large values of N_{tr} and g_{diff} no lasing is obtained, i.e. the laser is 'off'. There is an intermediate region where self-sustained pulsation can be observed. The results are depicted in Fig. 8 for four currents I_g. For both $I_g = 60$ mA (Fig. 8*a*) and $I_g = 200$ mA (Fig. 8*c*) self-pulsation occurs. As we will see later, the self-pulsation for the two currents is of a different type. For the larger current, the region of self-pulsating behaviour is very large. No self-pulsation was found for $I_g = 100$ mA and $I_g = 150$ mA (Fig. 8*b*).

To generate optical pulses, I_g, N_{tr} and g_{diff} must be adjusted such that the laser is 'off' without injecting current into the phase section I_{ph}. Moreover, for optimum operation, a region with self-pulsating behaviour should be

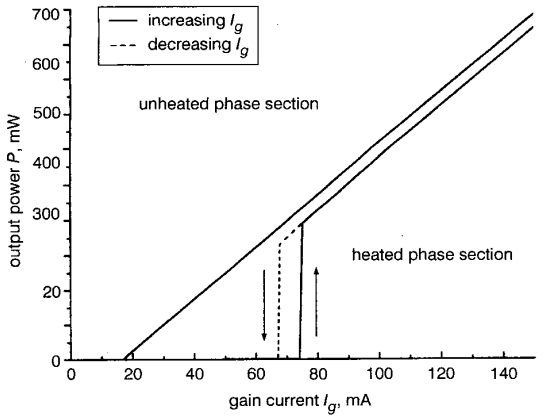

Fig. 7 *Calculated output power P against current I_g through the gain section*

Unheated phase section: $g_{diff} = 24 \times 10^{-18}$ cm^2, $N_{tr} = 0.8 \times 10^{18}$ cm^{-3}
Heated phase section: $g_{diff} = 125 \times 10^{-18}$ cm^2, $N_{tr} = 2.5 \times 10^{18}$ cm^{-3}

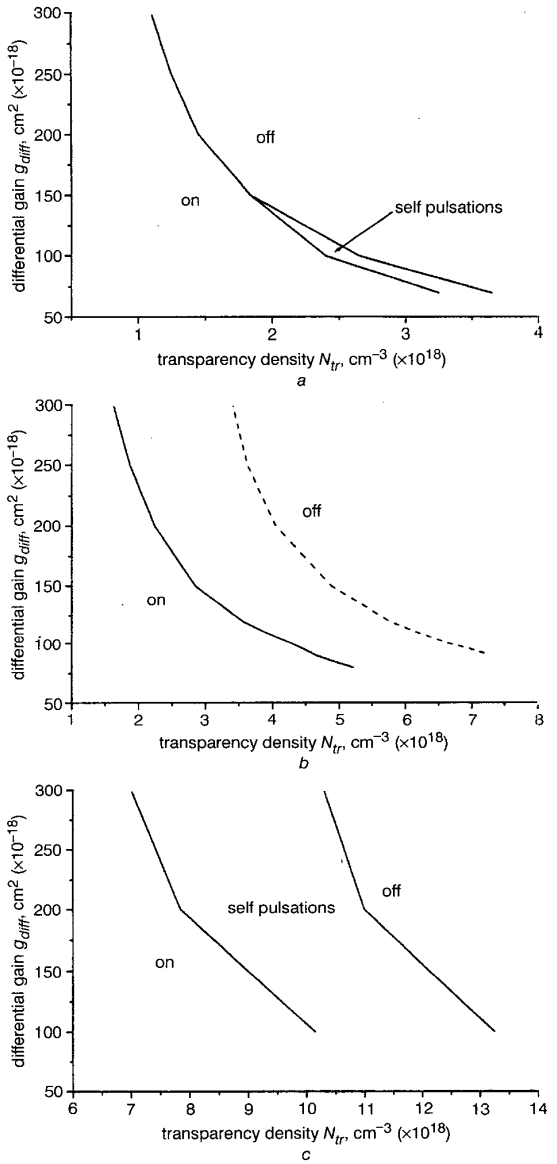

Fig. 8 *Calculated stationary stability diagrams for different gain currents*

a $I_g = 60$ mA
b $I_g = 100$ mA (solid line) and $I_g = 150$ mA (dashed line)
c $I_g = 200$ mA

located nearby, and the repetition frequency of I_{ph} should be near the frequency of self-pulsation.

5 Dynamic simulation

5.1 Self-pulsation

The generation of optical pulses with a given repetition frequency by injecting a modulated current into the phase section is facilitated by the occurrence of a self-pulsating behaviour. Therefore, we investigated the self-pulsation in more detail.

Self-pulsation for a gain current $I_g = 200$ mA (compare with Fig. 8*c*) is shown in Fig. 9. The pulsation frequency of 1.86 GHz is very stable. However, the peak power which reaches several watts fluctuates from pulse to pulse. The pulse width (FWHM) is typically 15–25 ps. In Figs. 10*a*, 10*b* and 10*c* the corresponding axial distribution of carrier density and right- and left-travelling optical power, respectively, is depicted for different points of time. It is assumed that the front facet with $R_f = 0.1$ is located at $z = 0$. In the following we will describe the temporal behaviour of the different axial distributions in more detail.

Some time after a light pulse is generated the carrier density in the whole gain section increases, because carriers are steadily injected and there is no stimulated recombination because the optical power is almost zero. During the same time, the carrier density in the phase section first decreases due to non-radiative and spontaneous radiative recombination, because there is no external supply of carriers ($\Delta t = +58 \ldots -142$ ps). If the carrier density is high enough (at $\Delta t = -42$ ps), the right-travelling field increases (see Fig. 10*b*) owing to the amplified spontaneous emission. Because most of the phase section is below transparency there is no feedback from the DBR. However, by the interband absorption of the photons excess carriers are generated first in the part adjacent to the gain section. This leads to an increase of the carrier density there and hence to a decrease of the absorption. Something like a 'transparency front' can be observed. At the same time, the carrier density in the gain section adjacent to the phase section decreases owing to stimulated recombination (spatial holeburning). At $\Delta t = -16$ ps, the phase section is almost transparent and the DBR starts to have an effect. From Fig. 10*c* it can be seen that a left-travelling field evolves. The left-travelling field which is created by the reflection of the large right-travelling field at the DBR is further exponentially amplified owing to the high carrier density in the gain section (see Fig. 10*c*: note the logarithmic scale of the power axis). This results in a light pulse emitted at the front (left) facet ($\Delta t = 0$). Because at the front facet some part of the left-travelling field is reflected back into the cavity and because the carrier density is still large, a few further small pulses with rapidly decreasing amplitude are emitted. At this point, the carrier densities in the gain and phase sections reach a minimum and a maximum, respectively, and start to increase and decrease, respectively.

The fingered power pattern seen especially in Fig. 10*b* is caused by the superposition of several longitudinal modes. This fact is supported by the optical spectrum calculated within a temporal interval of 260 ps presented in Fig. 11.

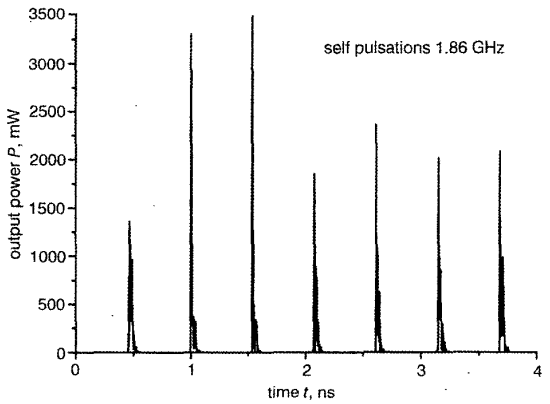

Fig. 9 *Calculated self-sustained pulsation for $I_g = 200$ mA*
Phase section: $g_{diff} = 125 \times 10^{-18}$ cm^2, $N_{tr} = 12.5 \times 10^{18}$ cm^{-3}

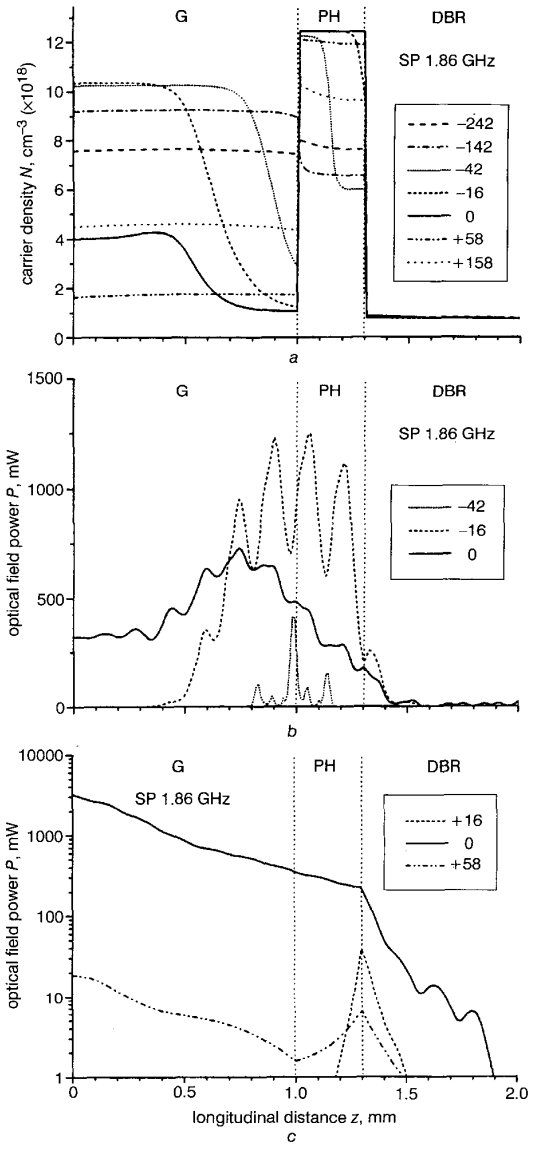

Fig. 10 *Axial profiles of the carrier density and the optical power at different points of time of a self-pulsation period for $I_g = 200$ mA*
The numbers denote the time in ps before (−) or after (+) the peak of the pulse. g_{diff} and N_{tr} are the same as in Fig. 9
a Carrier density
b Right travelling power
c Left travelling power. Note the logarithmic scale of the ordinate

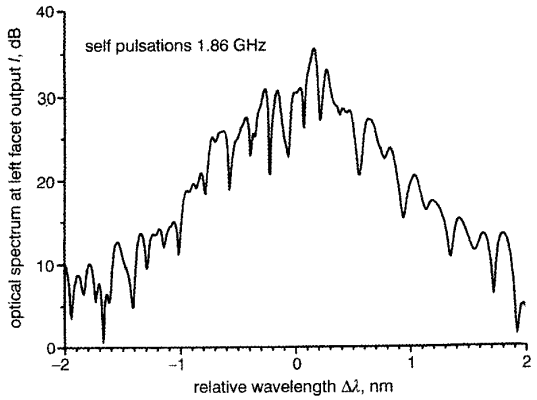

Fig. 11 *Calculated optical spectrum of a single self-pulsation for $I_g = 200$ mA*
g_{diff} and N_{tr} are the same as in Fig. 9

It exhibits several peaks about 0.1 nm apart which corresponds to the spacing of the modes of a Fabry–Perot cavity

$$\Delta\lambda_{FP} = \frac{\lambda^2}{2L_{eff}\, n_g} \tag{7}$$

with an effective cavity length $L_{eff} = 1.4$ nm (including a penetration depth into the DBR). Hence we conclude that the self-pulsation occurring for large currents through the gain section and having smaller repetition frequency is multi-moded.

Fig. 12 shows an example of self-pulsation occurring at a lower current $I_g = 60$ mA. The frequency of this self-pulsation is now about 3.1 GHz. The pulse shape and peak power do not change from pulse to pulse, in contrast to Fig. 9. However, the peak power is now an order of magnitude smaller. The pulse width (FWHM) is nearly 35 ps. The corresponding axial carrier density and power distributions are depicted in Fig. 13.

We find in principle the same behaviour of the carrier densities and the optical fields as described above. However, there are various differences. The carrier density in the phase section does not decrease so much after the pulse is emitted. The 'transparency front' is not so clearly seen. The spatial holeburning in the gain section is much weaker. The optical field distribution shows clearly an

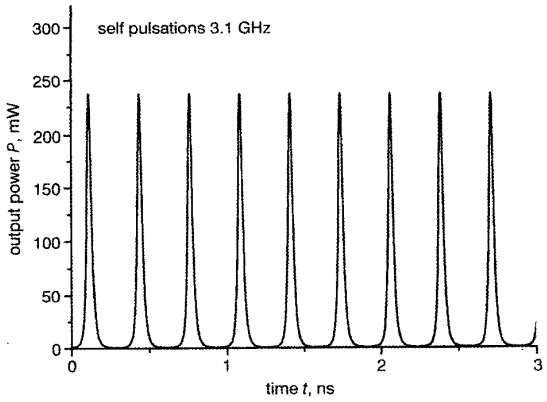

Fig. 12 *Calculated self-sustained pulsations for $I_g = 60$ mA*
Phase section: $g_{diff} = 100 \times 10^{-18}$ cm^2, $N_{tr} = 4.8 \times 10^{18}$ cm^{-3}

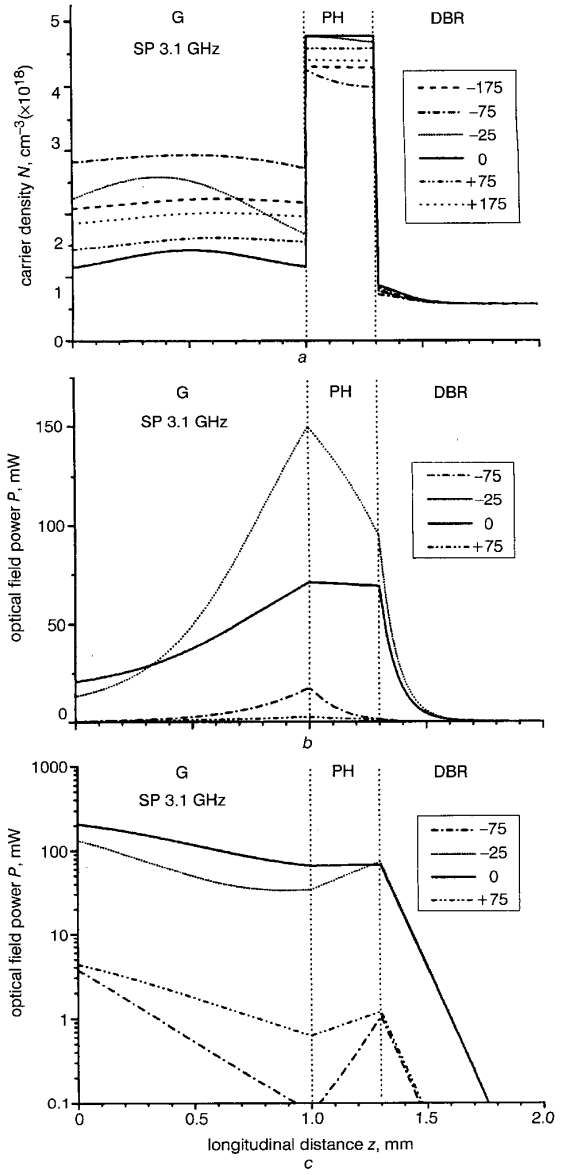

Fig. 13 *Axial profiles of the carrier density and the optical power at different points of time of a self-pulsation period for $I_g = 60$ mA*
The numbers denote the time in ps before (−) or after (+) the peak of the pulse. g_{diff} and N_{tr} are the same as in Fig. 12
a Carrier density
b Right travelling power
c Left travelling power. Note the logarithmic scale of the ordinate

exponential profile at low power and a more linear axial dependence at high power without any patterned structure. Obviously this is a single-moded self-pulsation, which is revealed by a look at the optical spectrum depicted in Fig. 14. There is only one peak located near $\Delta\lambda = 0$ (the maximum of the DBR spectrum). The spectral width (FWHM, 3 dB decrease) is around 0.1 nm.

To conclude this Section, we have found two types of self-pulsation. For small currents through the gain section and weaker heating there is a very regular single-moded self-pulsation with repetition rates of several GHz and peak powers of several hundreds of mW. For very large currents I_g and stronger heating there is multi-moded self-pulsation

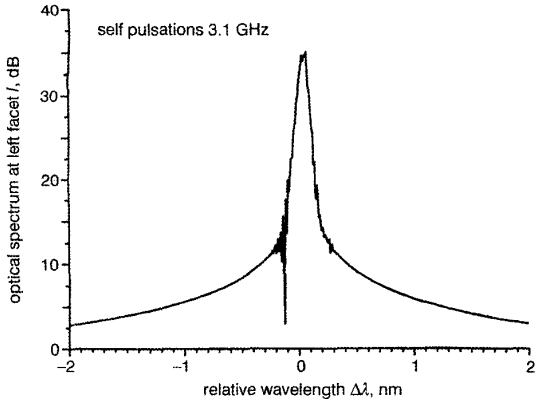

Fig. 14 *Calculated optical spectrum of a single self-pulsation for $I_g = 60$ mA*

g_{diff} and N_{tr} are the same as in Fig. 12

with smaller repetition rates but with a very high peak power of several W which fluctuates, however, from pulse to pulse.

5.2 Generation of optical pulses by injecting a modulated phase current

The controlled generation of short optical pulses can be realised by the injection of small current pulses I_{ph} through the p-n junction of the phase section. The current pulse leads to an increase of the carrier density and hence to a decrease of absorption there. Optical pulses are generated as described above in the case of self-pulsation but now the carrier density in the phase section is, at least partially, caused by the injected current I_{ph} and not by the interband absorption of photons alone.

Fig. 15*a* shows a simulation for a sinusoidal modulated current I_{ph} with a frequency of 312 MHz and an amplitude of 30 mA and the resulting temporal evolution of the output power for $I_g = 60$ mA. After the emission of a first short and strong pulse there is a big shoulder with an even smaller pulse at the end. Here, the current pulses are too long so that the laser is able to approach the stationary behaviour. Fig. 15*b* shows experimentally observed pulses obtained with similar modulation of the current through the phase section. The overall agreement with the theoretical pulse trace is very good, except that the small final pulse is missing.

Fig. 16*a* shows calculated light pulses with a repetition frequency of exactly 3 GHz. A zoom into a temporal interval of 330 ps is in shown in Fig. 16*b*, where additionally the corresponding current pulse through the phase section is depicted. The amplitude of the current pulse I_{ph} is only 30 mA, whereas the current through the gain section is $I_g = 100$ mA. The delay time between the maximum of I_{ph} and the maximum of the light pulse is about 50 ps. The width of the light pulse (FWHM) is about 30 ps. The temporal evolution of the axial profiles of carrier density and optical fields exhibits in principle the same behaviour as for the single-moded self-pulsation. The increase of the carrier density in the phase section up to

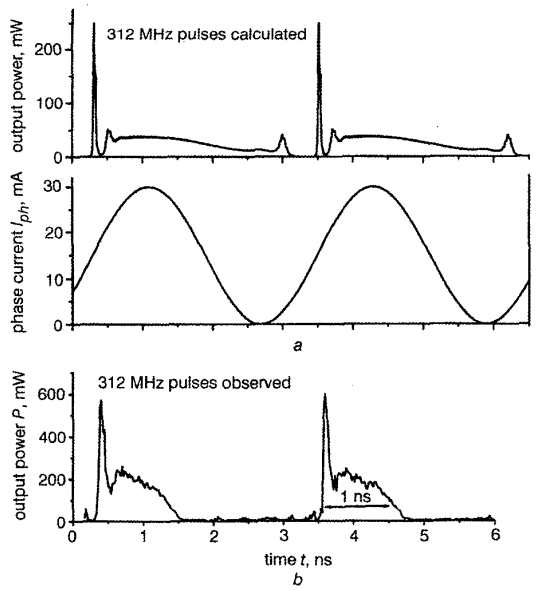

Fig. 15 *Optical pulses generated by a current I_{ph} which is modulated with a frequency of 312 MHz*

Both the gain and phase section are heated
a Calculated pulses for $I_g = 60$ mA. In the phase and Bragg sections: $g_{diff} = 175 \times 10^{-18}$ cm^2, $N_{tr} = 3.4 \times 10^{18}$ cm^{-3}. In the lower part of Fig. 15*a* the corresponding phase current pulses are shown. The sinusoidal pulse shape is nearly the same as in the experiment
b Measured pulses, $I_g = 500$ mA

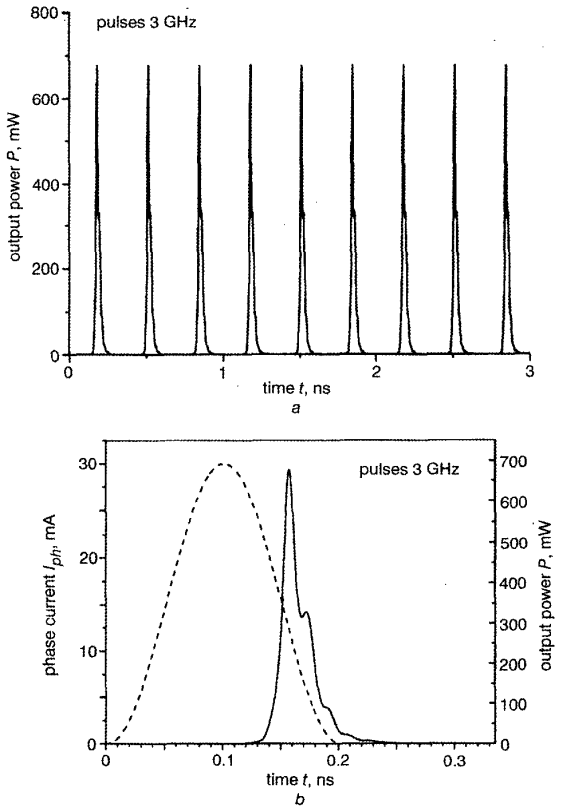

Fig. 16 *Calculated optical pulses generated by a current I_{ph} which is sinusoidally modulated with a frequency of 3 GHz*

Phase section: $g_{diff} = 100 \times 10^{-18}$ cm^2, $N_{tr} = 7.8 \times 10^{18}$ cm^{-3}
a Pulse train over 3 ns
b —— single optical pulse
- - - phase current I_{ph}

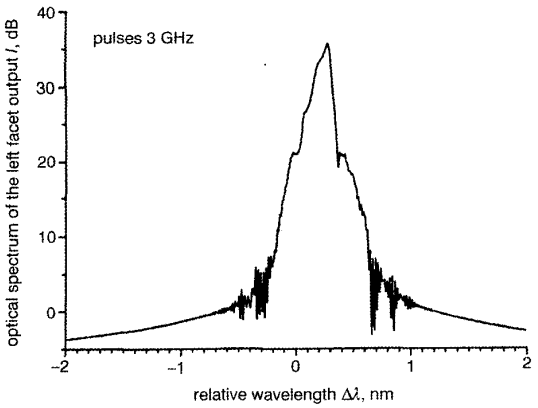

Fig. 17 *Optical spectrum of the light pulse in Fig. 16b*
The parameters are the same as in Fig. 16

the transparency carrier density N_{tr} is now partially caused by the injected current.

Nevertheless the interband absorption of the photons and subsequent generation of carriers in the phase section plays an important role, especially at low modulation frequencies. The phase current is then triggering the 'virtual' self-pulsations. At high modulation frequencies the phase current dominates more and more the increase of the carrier density which becomes more and more homogeneous. The amplitude of the modulated phase current must then be increased to achieve stable pulse operation.

The calculated optical spectrum of the light pulse of Fig. 16*b* is given in Fig. 17. The optical spectrum exhibits only one big peak, but it is broader than that shown in Fig. 14. The spectral width is around 0.2 nm. The reason is the higher current I_g, which leads to a larger change of the carrier density in the gain section during the pulse and hence to a larger chirp via the dependence of the refractive index on the carrier density (proportionality factor α_H). Additionally, owing to the higher carrier density in the gain section a few longitudinal side modes may possibly contribute to the pulse.

The product of the temporal width and the spectral width of these pulses is about $\Delta T \cdot \Delta f \simeq 1.8$. It exceeds the theoretical limit for a Gaussian pulse of [19]

$$\Delta T \cdot \Delta f = \frac{2 \ln 2}{\pi} = 0.44 \qquad (8)$$

by a factor of 4. The pulse energy is about 16 pJ.

6 Conclusions

We have demonstrated both experimentally and theoretically that three-section DBR lasers, where the active layer extends over all sections, exhibit switching behaviour, hysteresis phenomena and self-sustained pulsation. These phenomena are caused by the saturable interband-absorption within the active layer of the passive sections. Based on these results, it has been shown that optical pulses with high peak power (above 1 W), small pulse width (below 50 ps) and repetition rates in the GHz range can be generated by an appropriate heating of the phase section and by injecting small current pulses there.

The theoretical simulations were performed with the LDSL code which solves numerically the travelling wave equations and a rate equation for the carrier density including the stimulated generation-recombination term. The agreement with the experimental results is very satisfying. The heating of the phase section is simulated by an appropriate choice of the parameters determining the optical gain or absorption, respectively. The theoretical model will allow us to optimise the longitudinal geometry of the device and internal parameters with respect to peak power, pulse energy, pulse width and repetition frequency.

7 Acknowledgments

The authors are grateful for the financial support of the Deutsche Forschungsgemeinschaft (DFG) under the project KL 923. They are indebted to M. Radziunas (WIAS Berlin) and H.-J. Wünsche (HU Berlin) for providing the LDSL code.

8 References

1 VASILI'EV, P.P.: 'High-power high-frequency picosecond pulse generation by passively Q-switched 1.55 μm diode lasers', *IEEE J. Quantum Electron.*, 1993, **29**, pp. 1687–1692
2 SARTORIUS, B., MÖHRLE, M., REIHCHENBACHER, S., PREIER, H., WÜNSCHE, H.-J., and BANDELOW, U.: 'Dispersive self-Q-switching in self-pulsating DFB lasers', *IEEE J. Quantum Electron.*, 1997, **33**, pp. 211–218
3 AVRUTIN, E.A.: 'Analysis of spontaneous emission noise in self-pulsating laser diodes', *IEE Proc., Optoelectron.*, 1993, **140**, pp. 16–20
4 CARR, T.W., and ERNEUX, T.: 'Dimensional rate equations and simple conditions for self-pulsing in laser diodes', *IEEE J. Quantum Electron.*, 2001, **37**, pp. 1171–1182
5 RADZIUNAS, M., WÜNSCHE, H.-J., SARTORIUS, B., BROX, O., HOFFMANN, D., SCHNEIDER, K.R., and MARCENAC, D.: 'Modeling self-pulsating DEB lasers with an integrated phase tuning section', *IEEE J. Quantum Electron.*, 2000, **36**, pp. 1026–1034
6 HOFMANN, L., KLEHR, A., BUGGE, F., WENZEL, H., SMIRNITSKI, V., SEBASTIAN, J., and ERBERT, G.: '180 mW DBR lasers with first-order gratings in GaAs emitting at 1062 nm', *Electron. Lett.*, 2000, **36**, pp. 534–535
7 KLEHR, A., BUGGE, F., ERBERT, G., HOFMANN, L., KNAUER, A., SEBASTIAN, J., SMIRNITSKI, V.B., WENZEL, H., and TRÄNKLE, G.: '300 GHz continuously tunable high power three section DBR laser diode at 1060 nm', *Inst. Phys. Conf. Ser.*, 2000, **166**, pp. 383–386
8 KLEHR, A., HASLER, K.-H., WENZEL, H., and ERBERT, G.: 'Generation of high-power pulses in the GHz range with three-section DBR lasers', *Proc. SPIE-Int. Soc. Opt.*, 2002, **4651**, to be published
9 DAVIS, M.G., and O'DOWD, R.F.: 'A new large-signal dynamic model for multielectrode DFB lasers based on the transfer matrix method', *IEEE Photonics Technol. Lett.*, 1992, **4**, pp. 838–840
10 ZHANG, L.M., and CAROLL, J.E.: 'Large-signal dynamic model of the DFB laser', *IEEE J. Quantum Electron.*, 1992, **28**, pp. 604–611
11 LOWERY, A.J., KEATING, A., and MURTONEN, C.N.: 'Modeling the static and dynamic behavior of quarter-wave-shifted DFB lasers', *IEEE J. Quantum Electron.*, 1992, **28**, pp. 1874–1883
12 TSANG, C.F., MARCENAC, D.D., CAROLL, J.E., and ZHANG, L.M.: 'Comparison between 'power matrix model' and 'time domain model' in modelling large signal responses of DFB lasers', *IEE Proc., Optoelectron.*, 1994, **141**, pp. 89–96
13 KIM, B.-S., CHUNG, Y., and LEE, J.-S.: 'An efficient split-step time-domain dynamic modeling of DFB/DBR laser diodes', *IEEE J. Quantum Electron.*, 2000, **36**, pp. 787–794
14 WÜNSCHE, H.-J., BANDELOW, U., WENZEL, H., and MARCENAC, D.D.: 'Self pulsations by mode degeneracy in two-section DFB lasers', *Proc. SPIE-Int. Soc. Opt. Eng.*, 1995, **2399**, pp. 195–206
15 CARROLL, J.E., WHITEAWAY, J.E.A., and PLUMB, D.: 'Distributed feedback semiconductor lasers' (IEE, London, 1998, 1st edn.)
16 RADZIUNAS, M.: 'LDSL documentation'. WIAS, Weierstrass Institut für angewandte Analysis und Stochastik, Berlin, Germany, 2000
17 ELLMERS, C., GIRNDT, A., HOFMANN, M., KNORR, A., RÜHLE, W.W., JAHNKE, F., KOCH, S.W., HANKE, C., KORTE, L., and HOYLER, C.: 'Measurement and calculation of gain spectra for (GaIn)As/(AlGa)As single quantum well lasers', *Appl. Phys. Lett.*, 1998, **72**, pp. 1647–1649
18 BANDELOW, U., WÜNSCHE, H.-J., and SARTORIUS, B.: 'Dispersive self Q-switching in DFB lasers: theory versus experiment', *IEEE J. Sel. Top. Quantum Electron.*, 1997, **3**, pp. 270–278
19 BUUS, J.: 'Single frequency semiconductor lasers', Tutorial texts in optical, engineering (SPIE, Washington, 1991), Vol. TT-5